Journal of Engineering Mathematics (2006) 54: 261–271
DOI 10.1007/s10665-005-9029-7

The transfer of fibres in the carding machine

M.E.M. LEE[1,*] and H. OCKENDON[2]
[1]*BP Institute for Multiphase Flow, University of Cambridge, Madingley Road, Cambridge, CB3 0EZ, UK (E-mail: michael@bpi.cam.ac.uk);* [2]*OCIAM, Mathematical Institute, 24-29 St. Giles', Oxford, OX1 3LB, UK (E-mail: ockendon@maths.ox.ac.uk)*

Received 14 February 2005; accepted in revised form 13 December 2005 / Published online: 21 February 2006

Abstract. The problem of understanding the transfer of fibres between carding-machine surfaces is addressed by considering the movement of a single fibre in an airflow. The structure of the aerodynamic flow field predicts how and when fibres migrate between the different process surfaces. In the case of a revolving-flats carding machine the theory predicts a "strong" aerodynamic mechanism between taker-in and cylinder and a "weak" mechanism between cylinder and removal cylinder resulting in effective transfer in the first case and a more limited transfer in the second.

Key words: carding machine, fibre transport, tethered fibres, transfer mechanism

1. Introduction

1.1. Background

The fundamental operations of yarn manufacture are carding, drawing, twisting and spinning. Carding transforms the raw material, such as cotton, wool or polyester fibres, into a smooth coherent web; by disentangling and ordering the fibres and eliminating unwanted materials. Although manufacturing technology has improved the speed and efficiency of the process, the underlying principles have not changed for over 100 years. Originally the process was done by hand but now machines use huge arrays of hooks that tether and tease fibres or tufts at speeds of up to 100 m/s.

In modern carding machines, as shown in Figure 1, fibres essentially come into contact with hooks distributed on rapidly rotating cylinders and quasi-stationary flat plates. The first of the three cylinders is called the "taker-in", and this introduces the initially highly tangled fibres, labelled the "lap", into the carding machine. The hooked flat plates, known simply as "flats", adjacent to the largest cylinder, known as the "cylinder", act to break down and tease tufts into individual fibres. This leads to the formation of a smooth coherent web, called the "sliver", by the transferal of individual fibres from the main cylinder to the removal cylinder, known as the "doffer". In order to produce yarns, a number of further "macroscopic" deformations are applied to the sliver, such as transverse compression, stretching and twisting, but the physical properties of the resulting yarn depend critically on the formation of cohesive structures during the carding process.

There are two regions in a short-staple carding machine where fibres are "stripped" or transferred from one rotating cylinder to another: taker-in to cylinder and cylinder to doffer. Experience shows that virtually all fibres successfully migrate from taker-in to cylinder

*Corresponding author.

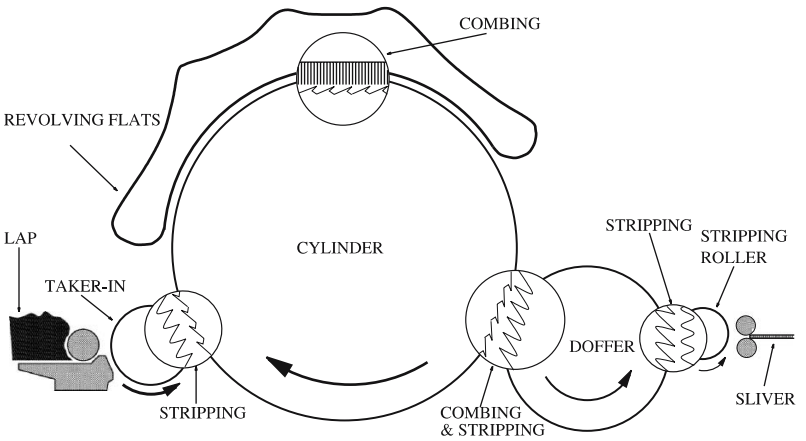

Figure 1. A diagram of a revolving-flats, short staple, carding machine.

whereas there is a less successful migration between cylinder to doffer. The main aim of this paper is to propose a mechanism for each transfer which explains this discrepancy.

The most obvious difference in the two fibre-transfer regions is the relative speed of the adjacent cylinders. Typically on a revolving-flats carding machine, the surface speed of the taker-in is 10 m/s, the cylinder is 35 m/s and the doffer is 1 m/s. The approximate hook heights on the taker-in and cylinder are 5 mm and are spaced at 6 and 15 hooks per square centimeter, respectively, whereas the doffer hooks are several times larger, and the gap between the hook tips varies but is no more than a few millimeters.

Although, initially many of the fibres are entangled, one can expect to find individual fibres throughout the process and by the time the textile has reached the end of the revolving-flats the tufts will be broken down into individual fibres; see [1]. Mathematical models for teasing entangled textile fibres are presented in [2, 3]. For groups of many entangled fibres, one would expect the faster cylinder to grab and remove tufts off the taker-in; the hooks on the taker-in are not directed to oppose this motion. However at the doffer, the material must transfer from the faster to the slower cylinder and the hooks on the doffer are, at first sight, pointing in the wrong direction. A model describing the journey of a single fibre in the carding machine is of particular importance, and the work in this paper goes some way to understanding this process.

1.2. Objectives

Understanding the mechanisms for fibre transfer between carding surfaces, will provide much needed insight into general fibre dynamics during the process, machine design and process-control optimisation, and the formation of the sliver. We will model the behaviour of a single fibre in the transfer regions of a carding machine, and these results could easily be extended to consider many fibres in a dilute suspension.

The approach of the work in this paper is in some sense a natural extension of the static analysis completed in [4], which considers frictional forces acting on a single fibre in tension, held by two hooks on opposing carding surfaces. The question this paper attempts to answer is: "When does this scenario occur and, in particular, how are fibres that are tethered to a hook on one carding surface presented to the hooks on another carding surface?"

A dimensional analysis shows that the dominant forces acting on a fibre are due to aerodynamic drag, which is contrary to current theories that suggest a centrifugal-force-driven

transfer (a review of these is presented in [5]). The aerodynamics in the carding machine involves complicated high-Reynolds-number flows generated by rapidly rotating, hooked cylinders, which are certainly turbulent in some regions. High-speed photographic observations near the doffer and cylinder, just after the transfer region, are presented in [6], and the experimental findings suggest that the flow is unsteady and probably turbulent. However, we will use a global inviscid model that can be considered as either the mean turbulent flow or the outer regime of a laminar boundary-layer flow to predict the aerodynamics in the transfer regions, which can then be used to determine the dynamics of tethered fibres. Our theory predicts two aerodynamic mechanisms that explain why the transfer rates between taker-in to cylinder and cylinder to doffer are very different.

2. Fibre model

In this section we derive the forces acting on a single fibre in a given airflow. We consider a fibre attached to a hook on a cylinder and take axes fixed in the cylinder as shown in Figure 2. These axes are rotating with angular velocity $\boldsymbol{\Omega}$ and the fibre is tethered at a radial distance of r_c. A dimensional analysis of the governing equations allow us to determine the dominant mechanisms for fibre transfer. Initially the equations will include effects due to linear and rotational acceleration of the fibre, drag and elasticity of the fibre.

Short wool, polyester and cotton are typical textiles that are carded in revolving-flats machines. They share a number of physical characteristics, the most obvious being that they all have small aspect ratios, $\epsilon = \frac{a}{l} \ll 1$, where a is the average diameter and l the average length of a fibre; polyester fibres are typically 6 micron in diameter and 4 cm in length. Therefore, we can approximate a fibre by its centre-line $\boldsymbol{R}(s,t) = (x(s,t), y(s,t), z(s,t))^T$, using s for arc length along the fibre and t for time. The coordinates (x, y, z) represent a local frame of reference for a fibre attached to one of the cylinders, where $\boldsymbol{R}(0,t) = 0$ is the point at which the fibre is tethered by a hook.

2.1. Drag on a fibre

Our approach assumes that the fibres are in a dilute suspension; this means that the presence and dynamics of the fibres do not affect the fluid flow. The air velocity $\boldsymbol{U}$ is given relative to the fibre velocity and due to axial symmetry we assume that the flow is two-dimensional.

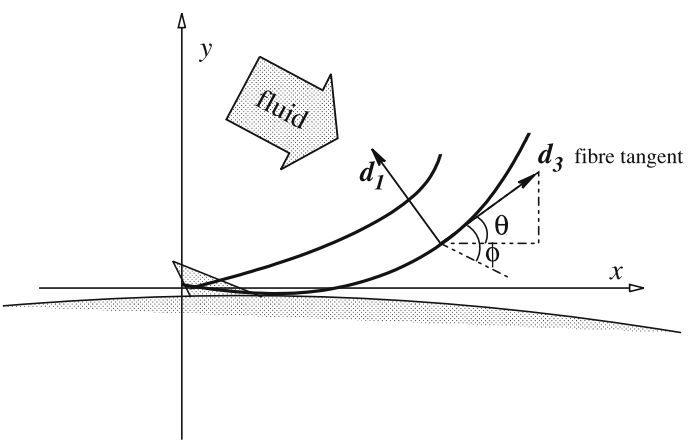

Figure 2. A diagram of a fibre tethered by a hook on a rotating cylinder.

The drag on a variety of different types of fibres were studied by Taylor [7]. This semi-empirical work measured the force acting on a fibre set obliquely to a stream of fluid, where the Reynolds numbers varied between 20 and 10^6. A range of drag laws are postulated for different fibre surfaces, such as smooth, rough and hairy. In practice the Reynolds number ($\mathrm{Re} = \frac{Ua}{\nu}$) for flow around a fibre in the carding machine can vary by three orders of magnitude, usually in the range $\frac{1}{2}$ to 10^2.

We define local orthonormal vectors for each point of a fibre with respect to the centre-line to be $(\boldsymbol{d_1}, \boldsymbol{d_3})$, where $\boldsymbol{d_1}$ is normal and is in the cross-sectional plane and $\boldsymbol{d_3}$ is the tangent; see Figure 2. Using $\phi(s,t)$ to represent the angle between the fibre's tangent and the fluid-stream direction, Taylor postulates that the drag term $\boldsymbol{D}$ per unit length for a hairy or bobbly surface, when $\mathrm{Re} \gg 1$, is

$$\boldsymbol{D} = c_F \frac{\rho_{\mathrm{air}} a U^2}{2} \left(-\sin\phi\, \boldsymbol{d_1} + \cos\phi\, \boldsymbol{d_3}\right), \tag{1}$$

where $|\boldsymbol{U}| = U$, $\phi \in [0, \frac{\pi}{2})$, ρ_{air} is the density of air and c_F is a parameter that is related to the specific surface properties and without loss of generality we will assume to be unity. Other drag laws for smooth and rough fibres in [7] involve nonlinear terms in $\sin\phi$.

Alternatively, for $\mathrm{Re} \ll 1$ we can apply classical Stokes flow in the neighbourhood of a fibre and the drag to leading order in ϵ for a smooth fibre is shown in [8] to be

$$\boldsymbol{D} = \frac{2\pi\mu U}{\log\frac{2}{\epsilon}} \left(-2\sin\phi\, \boldsymbol{d_1} + \cos\phi\, \boldsymbol{d_3}\right), \tag{2}$$

and μ is the viscosity of air. A number of other effects may also be considered from various analytical studies of slow flow past nematic objects, such as small deviations in surface geometry [9] and the effect of hydrodynamic interactions with other fibres [8].

To conclude, we see that the form of the drag term is similar in either case. On the taker-in $\mathrm{Re} \approx \mathcal{O}(10)$ and so we use the empirical approximation (1), whereas on the doffer the Reynolds number is $\mathcal{O}(1)$ so it is appropriate to use the Stokes drag given by (2). It turns out that the mechanism for transfer is not at all sensitive to which drag law is selected.

2.2. Internal fibre forces

Most fibres are not straight and even man-made fibres are deliberately crimped in order to produce more cohesive yarns. Although most textile fibres have bending moduli of the same order of magnitude, their natural shapes can vary considerably; see [10, Chapters 1 and 17]. For natural fibres a distribution of shapes occur due to the conditions during their formation whereas the uniform crimp in man-made fibres is regulated by machinery. Thus each fibre will have a natural curvature and given cross-sectional area. We begin by treating our fibre as a flexible, inextensible, circular, elastic rod and use Kirchhoff's equations to model its deformation [11, Chapter XVIII]. We write down the geometrical relationship, that the fibre tangent is normal to the cross-sectional plane,

$$\frac{\partial \boldsymbol{R}}{\partial s} = \boldsymbol{d_3}. \tag{3}$$

We define the stress resultant vector $\boldsymbol{N}(s,t)$ and the couple resultant vector $\boldsymbol{M}(s,t)$ to be

$$\boldsymbol{N}(s,t) = \sum_{i=1}^{3} N_i(s,t)\boldsymbol{d_i}(s,t), \quad \boldsymbol{M}(s,t) = \sum_{i=1}^{3} M_i(s,t)\boldsymbol{d_i}(s,t), \tag{4}$$

where N_1 and N_2 are the shear forces and M_1 and M_2 are the bending moments along the principal axes of the cross-sectional plane, while N_3 is the tensile force and M_3 is the twisting moment. Balancing forces and couples at each cross section in a rotating frame, with angular velocity $\boldsymbol{\Omega} = \Omega \boldsymbol{k}$, gives

$$\frac{\partial \boldsymbol{N}}{\partial s} + \boldsymbol{D} = A\rho\left(\frac{\partial^2 \boldsymbol{R}}{\partial t^2} + 2\,\boldsymbol{\Omega} \wedge \frac{\partial \boldsymbol{R}}{\partial t} + \boldsymbol{\Omega} \wedge (\boldsymbol{\Omega} \wedge (\boldsymbol{R} + r_c \boldsymbol{j}))\right), \tag{5}$$

$$\frac{\partial \boldsymbol{M}}{\partial s} + \frac{\partial \boldsymbol{R}}{\partial s} \wedge \boldsymbol{N} = \rho I \sum_{i=1}^{2}\left(\frac{\partial^2 \boldsymbol{d_i}}{\partial t^2} + 2\,\boldsymbol{\Omega} \wedge \frac{\partial \boldsymbol{d_i}}{\partial t} + \boldsymbol{\Omega} \wedge (\boldsymbol{\Omega} \wedge \boldsymbol{d_i})\right) \wedge \boldsymbol{d_i}, \tag{6}$$

where I is the coefficient of inertia, A is the cross-sectional area, and ρ is the density of the fibre. To complete the Equations (4)–(6) we use the Euler–Bernoulli constitutive law, which relates moments linearly with components of curvature (*i.e.*, the rotational strain):

$$\boldsymbol{M} = E I\,(\kappa_1 \boldsymbol{d_1} + \kappa_2 \boldsymbol{d_2}) + G J \kappa_3 \boldsymbol{d_3}; \tag{7}$$

here E is the Young's modulus, G is the shear modulus, J is the polar moment of inertia, and the κ_i's are the components of curvature. Equation (7) holds for a naturally straight rod; if a fibre is not uniformly straight, we need to interpret κ_i in (7) as the variations in curvature from the natural state.

In order to capture the important terms, we derive a dimensionless form to equations (5)–(6). Appropriate scalings for each variable are:

$$s = l\bar{s}, \quad \boldsymbol{R} = l\bar{\boldsymbol{R}}, \quad \kappa_i = \frac{\bar{\kappa}_i}{l}, \quad t = \frac{l}{\Omega r_c}\bar{t},$$
$$\boldsymbol{D} = D\bar{\boldsymbol{D}}, \quad \boldsymbol{N} = lD\bar{\boldsymbol{N}}, \quad \boldsymbol{M} = \frac{E I}{l}\bar{\boldsymbol{M}},$$

where the dimensionless quantities are denoted by an over-bar. The typical body force D represents the magnitude of the drag terms $\boldsymbol{D}$, which for Taylor drag will be $\rho_{\text{air}} a r_c^2 \Omega^2/2$ and for slow flow $2\pi\mu r_c \Omega / \log\frac{2}{\epsilon}$ as discussed in Section 2.1. Equations (5) and (6) become

$$\frac{\partial \bar{\boldsymbol{N}}}{\partial \bar{s}} + \bar{\boldsymbol{D}} = \Lambda_1\left(\frac{\partial^2 \bar{\boldsymbol{R}}}{\partial \bar{t}^2} + \delta \boldsymbol{k} \wedge \frac{\partial \bar{\boldsymbol{R}}}{\partial \bar{t}} + \delta \boldsymbol{k} \wedge \left(\boldsymbol{k} \wedge (\delta \bar{\boldsymbol{R}} + \boldsymbol{j})\right)\right), \tag{8}$$

$$\frac{\partial \bar{\boldsymbol{M}}}{\partial \bar{s}} + \Lambda_2 \frac{\partial \bar{\boldsymbol{R}}}{\partial \bar{s}} \wedge \bar{\boldsymbol{N}} = \Lambda_3 \sum_{i=1}^{2}\left(\frac{\partial^2 \boldsymbol{d_i}}{\partial \bar{t}^2} + \delta^2 \boldsymbol{k} \wedge (\boldsymbol{k} \wedge \boldsymbol{d_i}) + \delta \boldsymbol{k} \wedge \frac{\partial \boldsymbol{d_i}}{\partial \bar{t}}\right) \wedge \boldsymbol{d_i}, \tag{9}$$

respectively, where we have assumed that the wavelength of the crimp is comparable to the length of the fibre. This results in three important parameters:

$$\Lambda_1 = \frac{\rho A \Omega^2 r_c^2}{l\,D}, \quad \Lambda_2 = \frac{l^3 D}{E I}, \quad \Lambda_3 = \frac{\rho \Omega^2 r_c^2}{lE}, \quad \delta = \frac{l}{r_c}, \tag{10}$$

where Λ_1 represents fibre acceleration over drag, Λ_2 is drag over flexural rigidity, Λ_3 is the torque over elastic modulus and δ is the ratio of fibre length to cylinder radius. Since δ is always small, the additional terms in Equation (8), due to Coriolis and centrifugal accelerations, are small and we will ignore them from now on.

The above analysis leaves us with a number of parameters that will indicate the dominant mechanisms of fibre transport and will allow us to simplify the models accordingly. On both the taker-in and cylinder $\Lambda_2 \gg 1$ and $\Lambda_3 \ll 1$, and this suggests that in (9), the rotational

acceleration can be neglected and the fibre's elastic properties cannot compete with the drag induced by the fluid flow. Therefore the textile can be modelled as a string. Now Λ_1 varies between $\mathcal{O}(10^{-1})$ and $\mathcal{O}(1)$, so we regard it as small for the purpose of providing a simple illustration and proceed with a quasi-steady approximation. Since the $\mathrm{Re} = \mathcal{O}(10)$ based on the surface speeds of the cylinder or taker-in, we will also use the Taylor drag (1) in the following analysis. As explained above, the results are qualitatively the same if we use alternative drag law (2).

2.3. Equation for a quasi-steady tethered string

We now focus our attention on two-dimensional quasi-steady simulations with Taylor drag, as this could represent fibre dynamics on the taker-in and cylinder. The governing equations for deformations in an elastica, (8) and (9), where we now remove the over-bars, and neglect smaller quantities, reduce to

$$\frac{\partial \boldsymbol{N}}{\partial s} + \boldsymbol{D} = 0, \tag{11}$$

$$\frac{\partial \boldsymbol{R}}{\partial s} \wedge \boldsymbol{N} = 0. \tag{12}$$

Equation (12) implies that the stress resultant only has components in the direction of the tangent and we write $N_3 = T$ so that $\boldsymbol{N} = T(s,t)\boldsymbol{d_3}$. We use the inextensibility constraint to close the system of equations:

$$\boldsymbol{d_3} \cdot \boldsymbol{d_3} = 1. \tag{13}$$

The fibre equations incorporate a general fluid velocity $\boldsymbol{U} = (u, v)$, and

$$\phi(s) = \theta(s) - \arctan\left(\frac{u}{v}\right), \tag{14}$$

where θ is the angle between fibre tangent and the cylinder surface (see Figure 2). The dimensionless governing equations (11) now read:

$$\frac{\mathrm{d}T}{\mathrm{d}s} + (u^2 + v^2)\cos\phi = 0, \tag{15}$$

$$T\frac{\mathrm{d}\theta}{\mathrm{d}s} - \mathrm{sgn}(\phi)(u^2 + v^2)\sin\phi = 0, \tag{16}$$

$$\frac{\mathrm{d}x}{\mathrm{d}s} - \cos\theta = 0, \tag{17}$$

$$\frac{\mathrm{d}y}{\mathrm{d}s} - \sin\theta = 0. \tag{18}$$

It remains to apply boundary conditions, and we use the fact that the fibre is free at the non-tethered end $s = 1$ and fixed geometrically at the other end $s = 0$,

$$T(1) = 0, \quad x(0) = 0, \quad y(0) = 0. \tag{19}$$

The angle of the free end $\theta(1)$ needs to be found by solving the equation

$$\sin\phi(1) = 0, \tag{20}$$

which is due to the no-tension condition from (19) that would otherwise cause a singularity in (16). This leaves us with a fourth-order system of coupled ordinary equations (15)–(18) with four boundary conditions (19) and (20) to determine the position of a given fibre in a given flow (u, v).

3. Aerodynamics

We now turn our attention to the fluid flow. The Reynolds numbers of fluid flow in the machine vary from $\mathcal{O}(10^4)$ and $\mathcal{O}(10^6)$ and so we expect it to be turbulent. This can be modelled by an inviscid mean flow when the Reynolds stresses are small. If the flow is laminar, an inviscid approximation will also be adequate, except when close to the machine surfaces. We do not attempt to model the effect of the hooks but one expects that they act as vortex generators and would encourage turbulent behaviour.

To elucidate the basic flow structure we consider a simple two-dimensional incompressible, irrotational and inviscid flow. Transfer occurs in regions between two cylinders, c_+ and c_-, of radius r_+ and r_- counter-rotating with angular velocities $\mathbf{\Omega}_+$ and $\mathbf{\Omega}_-$ in close proximity to each other; see Figure 3. We prescribe no-penetration conditions and circulations Γ_+ and Γ_- around each drum. This is equivalent to placing a point vortex within each cylinder. Note that a cylinder, of radius r, rotating in an infinite fluid at high-Reynolds-number flow will eventually create a circulation $\Gamma = 2\pi r^2 \mathbf{\Omega}$ when rotating at angular velocity $\mathbf{\Omega}$ and thus $\Gamma_- = 2\pi \mathbf{\Omega}_- r_-^2$ and $\Gamma_+ = 2\pi \mathbf{\Omega}_+ r_+^2$ are plausible values to take.

There are a number possible flow topologies that can occur as a consequence of variations in the circulations Γ_+ and Γ_-. However, in the case of the carding machine, the larger cylinder c_+ is moving considerably faster than the smaller one c_- and so drives a rotational flow round both doffer and taker-in; the magnitude of Γ_+ will be much greater than the magnitude of Γ_-. However, the counter-rotation of c_- affects the flow in the gap between the cylinders. This situation is illustrated in Figure 3, with two stagnation points on the smaller, slower cylinder. The large cylinder will entrain fluid, some of which will be ejected onto the smaller cylinder, when approaching the nip-regions between the drums. We postulate that the airflow near the stagnation points is the critical area for fibre transport and different fibre-transfer mechanisms occur in going from the large and fast cylinder to a smaller slower cylinder or vice versa as described in the next two sections.

The flow illustrated in Figure 3 is a gross simplification and in reality will be modified by boundary-layer effects, the effect of the hooks and the presence of other machine surfaces, but the changes in the mean flow direction near a stagnation point will still occur and this is the mechanism that we need to effect transfer of fibres from one cylinder to another.

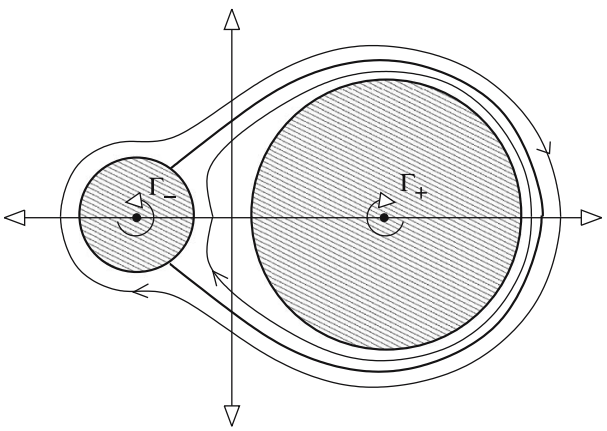

Figure 3. The flow topology for two neighbouring counter-rotating cylinders. The gap width between the cylinders is greatly exaggerated in this figure to allow the basic flow structure to be clearly illustrated.

4. Strong transfer

We use the term "strong transfer" to describe the process that occurs in going from the taker-in to the cylinder. In this section we describe a theoretical scenario that shows how single fibres will transfer, due to aerodynamic forces, without being in simultaneous contact with hooks on the taker-in and cylinder. This means that the transfer mechanism is purely aerodynamic and does not involve the cylinder and taker-in hook competition described by [4].

We consider the flow near the taker-in as a fibre is transported into the stagnation region, and assume that the flow is of the type illustrated in Figure 3, where two stagnation points reside on the taker-in. Figure 4(a) illustrates the flow near the stagnation points on the taker-in; both surfaces move from right to left in the diagram but the cylinder moves at greater velocity. We use a simplified flow containing two stagnation points in order to see how a fibre connected to a hook on the taker-in is affected by this type of flow. First, we introduce global coordinates (X,Y) where the stagnation points are placed at $X=\pm a$ on an infinite plate at $Y=0$; see 4(b). The complex potential for a particular flow field containing two stagnation points on $y=0$ is $w(z)=A_0\left(\frac{z^3}{3}-za^2\right)$, with components of velocity

$$u=A_0(X^2-Y^2-a^2), \quad v=-2A_0XY, \tag{21}$$

and the streamlines are also illustrated in Figure 4(b). This flow is used to simulate the motion of the fibre shown in Figure 5 using the quasi-steady model (15)–(20). The point at which the fibre is tethered $\boldsymbol{R}(s=0)=(X,Y_T)$, moves from right to left, so X decreases for some fixed Y_T.

As a fibre moves from the right to the first stagnation point at $X=a$, its displacement will not alter significantly nor will the aerodynamic forces lift the fibre away from the taker-in

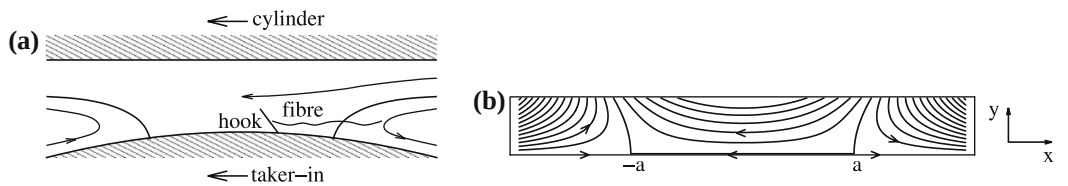

Figure 4. Flow for strong transfer. (a) Schematic diagram of the strong transfer region. (b) Stagnation flow streamlines.

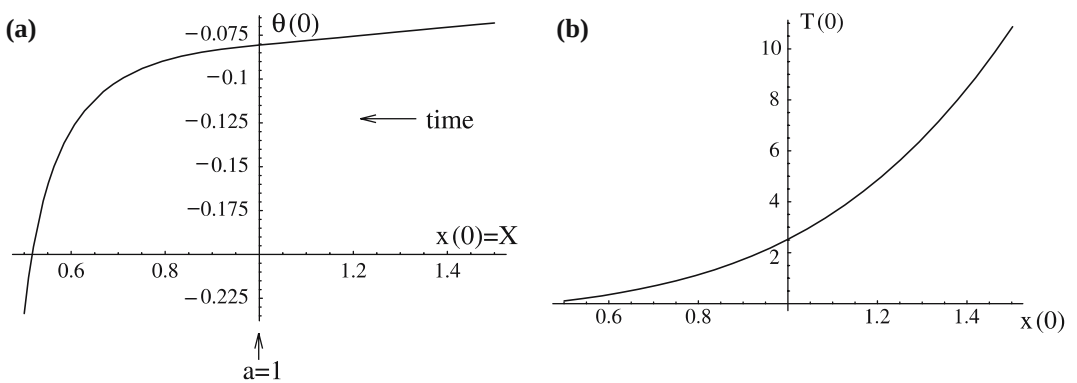

Figure 5. Strong transfer for stagnation point flow where $a=\pm1$; the tethered point Y_T moves from right to left, $x(0)=X$ decreasing from 1·5 to 0·5 and passes through the stagnation streamline near $X=1$. (a) Fibre angle at $s=0$ (b) Fibre tension at $s=0$.

surface. As the fibre moves past the stagnation streamline at $X \approx a$, the fluid begins to drag the fibre towards the cylinder surface. At this point in time the tethered angle $\theta(0)$ decreases more dramatically and the tension $T(0)$ tends to zero, making it more likely that the fibre-hook contact point will slip and the fibre will free itself from the hook altogether; see Figure 5. The fibre when free will be transported away from the surface at $Y = 0$ and will migrate to the cylinder, since in the case of negligible inertia it is known that a fibre will rapidly align with the flow [12].

5. Weak transfer

A weaker transfer occurs between the cylinder and doffer. The build-up of fibres on the cylinder has been studied in some detail, and it is observed that only a small proportion of the fibres on the cylinder are transferred from the cylinder to the doffer; see [5]. Although the flow regime is again assumed to be of the type illustrated in Figure 3, this time the fibres are on the cylinder while the stagnation points are on the doffer as shown in Figure 6(a). Note that the direction of the cylinder has been reversed for ease of comparison with the strong transfer mechanism. When a fibre is transported from right to left along the X-axis, the trailing ends of the tethered fibres will be dragged towards the doffer by the upward flow. The maximum altitude of the trailing end, depends on the locality of the neighbouring surface $Y = h_p$ and height of the tethered point $y(0) = Y_T$.

To illustrate this process, we calculate the position of a fibre tethered by hooks on the cylinder as it moves toward the doffer on which two stagnation points reside. We have chosen to use a stagnation point flow with a fixed semi-infinite plate at $Y = h_p$ and a parallel infinite plate at $Y = 0$, see diagram 6(b), as we are interested in the first stagnation point of the flow because it is in this region the airflow will lift the fibre toward the adjacent surface. The infinite lower plate represents the surface of the cylinder. If the high-Reynolds-number flow is laminar, the leading-edge region is predominantly governed by Euler's equations which match onto boundary layers on both plates. We will use an inviscid solution given by [13] for the flow and then solve Equations (14)–(20) for an inextensible fibre.

In Figure 7, we show quasi-steady animations of a fibre that moves underneath the stagnation point. We note that the hooks on the doffer will typically occupy the majority of the region $0 < Y < h_p$, and so in both cases shown there will be a good chance of interaction with the doffer hooks. It is not the case that all fibres that are presented will actually make contact with a hook, and to compute the likelihood of interaction one would need to consider the volume fraction of doffer hooks in the stagnation region. Once the fibres come into contact with a doffer hook, there will be a competition between the frictional properties of the doffer and cylinder hooks and this, along with the way the fibre is presented to the doffer hook, the

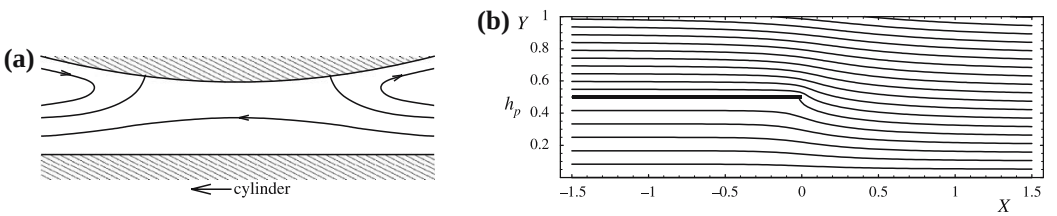

Figure 6. Flow for weak transfer. (a) Schematic diagram of the weak-transfer region. (b) Streamlines for parallel infinite and semi-infinite plates set at a distance $h_p = 0{\cdot}5$ apart.

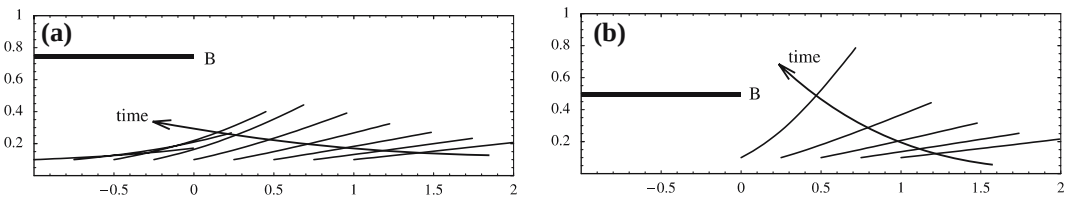

Figure 7. Displacements of a fibre attached at height $Y_T = 0{\cdot}1$ as it moves from the right towards the stagnation point B. Figure (b) includes the hooks to which the fibres are tethered.

changing angle of attachment $\theta(0)$ to the cylinder hook and the hook geometries will determine when transfer occurs. In the case of weak transfer, the static competition described by [4] will then be appropriate to complete the transfer model.

6. Conclusion

We have postulated a theory of how individual fibres behave in the carding machine. In a simple dimensionless analysis, we eliminated the possibility of centrifugally driven transfer theories, and highlighted the importance of aerodynamics within the carding process. Looking at the mean airflow, stagnation-point flows occur in the transfer regions between cylinders in the carding machine. These produce two very different transfer mechanisms near the leading stagnation point: the strong mechanism occurs between taker-in and cylinder where all fibres migrate to the cylinder surface as the tension holding the fibre to the hook decreases to zero and the weak mechanism between cylinder and doffer where only a proportion of fibres transfer to the doffer by slipping off one set of hooks and being caught or held by the other.

The experimental observations in [6] provide some evidence that supports our aerodynamically driven transfer mechanisms described above. Their observations focussed on the region between doffer and cylinder, just after the point where fibres transfer from cylinder to doffer. This coincides with the region close to the second stagnation point in Figure 6(a). Figures 11, 12 and 14 in [6] show fibres that have already transferred from cylinder to doffer, being entrained by the fluid away from the doffer surface back towards the cylinder. As the fibres are tethered to the doffer, a surface upon which stagnation points reside, the local fluid flow relative to the fibre will be similar to the strong-transfer-mechanism aerodynamics depicted in Figure 4, in particular the region close to the left stagnation point. The reason why there is far greater retention of fibres on the doffer, when compared to similar fluid-entrained dynamics on the taker-in, is the hook size and more importantly the angle; see Figure 1; the doffer hooks oppose the fibre motion away from the doffer surface.

The "micro-scale" work in this paper could be used to complement carding-machine models that employ "macroscopic" variables such as fibre density, and assume probabilistic transfer rates between carding surfaces, such as [14–17]. The "macroscopic" parameters within these models are chosen by comparison with experimental data. By using the simulations and models explored in this paper, we could relate the large-scale model parameters to hook geometry and density, fibre-hook friction, fibre length, cylinder geometry and linear surface speeds.

Acknowledgements

We wish to express our gratitude to the EPSRC (Grant GR/L62153) and Crosrol Ltd. who funded the interdisciplinary project through which this research was undertaken. We are

also grateful to Prof C. Lawrence, Dr. Abbas, Mr. B. Greenwood, Dr. C. Iype and Dr. M. Mahmoudi of the Department of Textile Industries at Leeds University and Dr. M. Jones of the School of Mathematics, University of Southampton for many useful discussions.

References

1. A. Dehghani, C.A. Lawrence, M. Mahmoudi, B. Greenwood and C. Iype, An assessment of changes in the state of fibre mass during the early stages of the carding process. *J. Textile Inst.* 91 (2000) 359–373.
2. M.E.M. Lee and H. Ockendon, A continuum model for entangled fibres. *Eur. J. Appl. Math.* 16 (2005) 145–160.
3. G. Kozyreff, M.E.M. Lee and H. Ockendon, Towards understanding the internal forces in a tuft of fibres. Submitted.
4. Y.A. Baturin, The load of the surfaces and the proportion of fibre transferred between the surfaces. *Technol. Textile Industry, U.S.S.R.* 4 (1964) 37–43.
5. C.A. Lawrence, A. Dehghani, M. Mahmoudi, B. Greenwood and C. Iype, Fibre dynamics in the revolving-flats card, part 1, a critical review. *AUTEX Res. J.* 1 (2000) 64–77.
6. A. Dehghani, C.A. Lawrence, M. Mahmoudi, B. Greenwood and C. Iype, Aerodynamics and fibre transfer at the cylinder-doffer interface. *J. Textile Inst.* 95 (2004) 35–49.
7. G.I. Taylor, Analysis of the swimming of long and narrow animals. *Proc. R. Soc. London A* 214 (1952) 158–183.
8. R.G. Cox, The motion of long slender bodies in a viscous fluid part 1. General theory. *J. Fluid Mech.* 44 (1970) 791–810.
9. G.K. Batchelor, Slender-body theory for particles of arbitrary cross-section in stokes flow. *J. Fluid Mech.* 44 (1970) 419–440.
10. W.E. Morton and J.W.S. Hearle, *Physical Properties of Textile Fibres*. London: William Heinemann (1975) 660 pp.
11. A.E.H. Love, *A Treatise on the Mathematical Theory of Elasticity*, 4th edn. Cambridge: Cambridge University Press (1927) 643 pp.
12. E.J. Hinch, The distortion of a flexible inextensible thread in a shearing flow. *J. Fluid Mech.* 74 (1976) 317–333.
13. M.A. Jones and F.T. Smith, Fluid motion for car undertrays in ground effect. *J. Engng. Math.* 45 (2003) 309–334.
14. A.S. Abhiraman and W. George, A new aspect of the stochastic nature of carding. *Textile Res. J.* 43 (1973) 452–467.
15. H.M. Gutierrez, J.P. Rust and A.F. Seyam, Modeling and simulation for control carding. *Textile Res. J.* 65 (1995) 638–643.
16. J.P. Rust and H.M. Gutierrez, Mathematical modeling and simulation for carding. *Textile Res. J.* 64 (1994) 573–578.
17. L.D. Wibberly and W.W. Roberts Jr., Modeling the diffusive transport of bulk fiber mass in a card. *Textile Res. J.* 67 (1997) 296–308.